This article has been accepted for publication in a future issue of this journal, but has not been fully edited. Content may change prior to final publication. Citation information: DOI 10.1109/ACCESS.2018.2829618, IEEE Access

Improved methodology to estimate the power transfer efficiency in an inductively coupled radio frequency ion source

Palak Jain, Mauro Recchia, Pierluigi Veltri, Marco Cavenago, Alberto Maistrello and Elena Gaio

***Abstract*—The ITER NBI includes an ion source which can produce D^- ion beams for 1 hour, accelerated at the energy of 1 MeV. An ion source consists of a 'driver' where the plasma is produced by the application of the radio frequency (RF) power to an inductive coil. This paper presents an improved methodology which provides an estimation of the power transfer efficiency to the plasma of the driver. The developed methodology is based on different mechanisms which are responsible for the plasma heating (ohmic and stochastic) and an electrical model describing the power transfer to the plasma. As a first approximation in a previous work, a transformer model was assumed as an electrical model. In this work, a main improvement is introduced based on the development of a multi-filament model which takes into account the mutual coupling between the RF coil, the plasma and the passive metallic structure. The methodology is applied to the NIO1, a flexible negative ion source, currently in operation at Consorzio RFX, Italy. The results from the two models – transformer and multi-filament are presented and compared in terms of plasma equivalent resistance and power transfer efficiency. It is found that results obtained from both the transformer and the multi-filament model follows the same trend in comparison with the applied frequency and the other plasma parameters like electron density, temperature and gas pressure. However, lower values of the plasma equivalent resistance and power transfer efficiency are observed with the multi-filament model. The multi-filament model reproduces a more realistic experimental scenario where the power losses due to the generation of the eddy currents in the metallic structure are considered.**

***Index Terms*— Power transfer, frequency variation, inductively coupled plasmas, stochastic heating, multi-filament model, ion sources, plasma equivalent resistance, efficiency.**

I. INTRODUCTION

SEVERAL studies are available in literature [1]–[9] which focus on the inductively coupled plasmas (ICPs). In an inductive discharge, the plasma is generated and maintained in a dielectric region (called driver) surrounded by a coil [1], [2]. Radio-frequency (RF) power continuously applied to the coil induces electric fields that partially ionize a gas inside the chamber and sustain a discharge. There is wide range of applications for ICPs such as for medical use, accelerator for high-energy particle physics and fusion plasma heating.

One such IC RF ion source [10] is the heart of Neutral Beam Injection (NBI) system required for plasma heating and current drive in ITER (International Thermonuclear Experimental Reactor) [11]. ITER requires two NBIs rated for a total power of 33 MW [12]. The ITER NBI is composed of an ion source (at 1 MHz) which can produce D^- ions for 3600 s to be accelerated up to the energy of 1 MeV and with a current of 40 A [12]. The principle concept behind these ion sources was developed at IPP, Garching in Germany where the most recent test facility is ELISE (Extraction from a Large Ion Source Experiment) [13], able to operate with both hydrogen and deuterium gas species and having half the size of the ITER NBI source [14]. To meet the challenging requirement for ITER, never achieved all together in a single device so far, the ITER neutral beam test facility (NBTF) called PRIMA, is under development in Padova, Italy. It includes two projects: MITICA (Megavolt ITER Injector and Concept Advancement) is the full scale prototype of the NBI for the ITER experiment and SPIDER (Source for Production of Ion of Deuterium Extracted from RF plasma) will focus on the development of the NBI ion source. In addition, to provide both a benchmark for the codes and a more flexible and accessible facility, a small ion source called NIO1 [15], [16] has been constructed at Consorzio RFX. NIO1 stands for (Negative Ion Optimization 1) with nominal H^- beam current of 130 mA at 60 keV and an operational frequency of 2 MHz.

One of the issues of the ion sources for these applications is the efficiency of the RF power transfer from the coil to the plasma in the driver region. A methodology has been developed and implemented in MATLAB® to estimate this efficiency; it is based on the description of different mechanisms responsible for the plasma heating (ohmic and stochastic) and of an electrical model responsible for the power transfer to the plasma [3]. The development of this model started from the classical method where the mutual coupling between the coil and the plasma is described by a transformer model [4]. This was the approach applied to the simplified driver of the ELISE ion source, characterized by a maximum power per driver of about 90 kW [3]. A significant limitation of the classical method is that it neglects the eddy currents generated in the metallic structures surrounding the driver region, thus the power fraction not absorbed by the

P. Jain, M. Recchia, P. Veltri, A. Maistrello and E.Gaio are with Consorzio RFX, Corso Stati Uniti, 4, 35127, Padova, Italy (e-mail: palak.jain@ igi.cnr.it, mauro.recchia@igi.cnr.it, pierluigi.veltri@igi.cnr.it, alberto.maistrello@igi.cnr.it and elena.gaio@ igi.cnr.it).

M. Cavenago is with INFN-LNL, Viale dell'Università 2, I-35020, Legnaro, Italy (e-mail: marco.cavenago@lnl.infn.it).

This article has been accepted for publication in a future issue of this journal, but has not been fully edited. Content may change prior to final publication. Citation information: DOI 10.1109/ACCESS.2018.2829618, IEEE Access

plasma. In our revised methodology, a first approach to account for the passive structure surrounding the driver region has been developed.

A further enhanced methodology is also presented in this paper; it includes some improvements, the main one consisting in the introduction of a multi-filament model which takes into account the mutual coupling between the plasma, the RF coil and the passive metallic structure. Hence, this model should be more capable of describing the real experimental conditions. Both the first and the improved methodologies are then applied to the NIO1 ion source, which is characterized by a maximum power of 2.5 kW on the driver. The effect of the applied frequency on the power transfer efficiency is analyzed, as done in [3], as it is an external parameter which can be selected and controlled. In the second part of the paper, the focus is more on the operating parameters of the NIO1 ion source at a working frequency of 2 MHz; in these specific operating conditions, the relative merit of the multi-filament model against the transformer one will be presented and discussed.

II. METHODOLOGY

The developed methodology can be applied to any IC RF ion source; a block diagram is given in Fig. 1. The first section within the light blue box is based on the simplified approach of steady state plasma and is a 0 D model. It is not based on kinetic or fluid numerical models.

The detailed description of the different sections of the methodology can be found in [3]. This paper briefly recalls its key points and presents three significant improvements incorporated within it. These improvements consists of the multi-filament model considered in step (h), the consideration of the geometric effects in the calculation of the skin depth in step (c and f) and the estimation of the electron temperature with the ion source in step (a) of the methodology in Fig. 1.

A. Input parameters

The first step in [3] was to choose the geometry of the source along with gas type and pressure, operational frequency and plasma parameters like electron density and temperature (step (a) in Fig. 1). The plasma parameters used in the MATLAB® code are independent quantities, i.e. they are not related to each other. In reality, the electron density is dependent on electron temperature and is also known to have a radial profile within the ion source [17]; however, we specify that the first approximation assumed in this methodology is to consider the electron density as a uniform and an independent parameter within the ion source. Therefore, the developed model is not self–consistent in this regard. In the last part of the paper, an attempt is reported to account for the non-flat density profile.

A.1. Estimation of plasma electron temperature

There is an attempt to make the developed methodology more self-consistent in such a way that the electron temperature profile is first estimated and then used as an input parameter for the methodology, contrary to what is done in the previously formulated methodology [3].

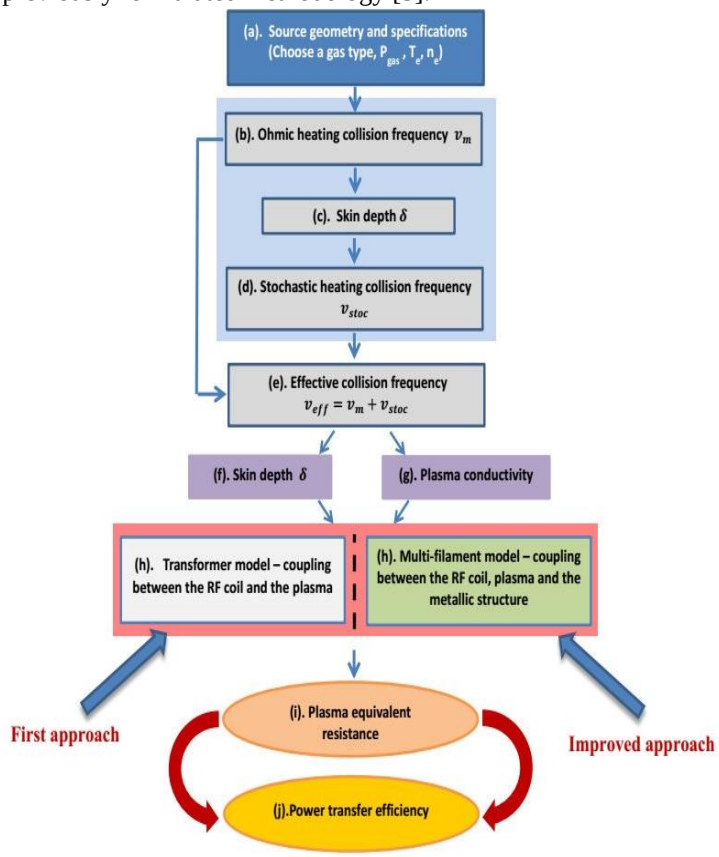

Fig. 1. Methodology to calculate the power transfer efficiency in an IC RF ion source

Following this path, a model is included which can calculate the electron temperature of the plasma within the driver region. Considering the plasma with the radius *a* and length *l*, the particle balance equation gives [1]

$$\frac{K_{iz}(T_e)}{u_B(T_e)} = \frac{1}{n_g d_{eff}} \tag{1}$$

Here, K_{iz} is the ionization rate constant, u_B is the Bohm velocity, (both K_{iz} and u_B are functions of electron temperature) n_g is the gas density calculated from the known gas pressure P_{gas} and gas temperature T_{gas} within the ion source, d_{eff} is the effective plasma size and is defined as

$$d_{eff} = \frac{1}{2}\frac{al}{ah_l + lh_a} \tag{2}$$

h_l and h_a are the edge to center density ratios [1]. By numerically solving equation (1), one can obtain the electron temperature as a function of P_{gas} and T_{gas}.

B. Description of the analytical model for the power deposition within the IC plasma sources

This part of the methodology is well described in detail in [3] and is highlighted with light blue box in Fig. 1. The main components of the analytical model are the ohmic and the stochastic heating which are the two important mechanisms leading to the deposition of the power within the plasma. With the input parameters (step (a)), the ohmic heating collision

This article has been accepted for publication in a future issue of this journal, but has not been fully edited. Content may change prior to final publication. Citation information: DOI 10.1109/ACCESS.2018.2829618, IEEE Access

frequency ν_m (step (b)) and the stochastic heating collision frequency ν_{stoc} (step (d)) are calculated.

The ohmic heating collision frequency ν_m is calculated by the sum of three different frequencies [1][3][18]: the electron-neutral elastic collision frequency ν_{en}^{p}, electron-neutral ionization collision frequency ν_{en}^{iz} and electron-ion collision frequency ν_{ei}^{p}. From this ν_m, the skin depth δ is estimated as described in equation (3),

$$\delta = \frac{c}{\omega_{p_e}} \left(\frac{2\left[1+\left(\frac{\nu^2}{\omega^2}\right)\right]}{y\left\{1+\left[1+\left(\frac{\nu^2}{\omega^2 y^2}\right)\right]^{\frac{1}{2}}\right\}} \right)^{\frac{1}{2}} \tag{3}$$

where, $y = 1 + x\left(1+\left(\frac{\nu^2}{\omega^2}\right)\right)$ and $x = \left(\frac{c}{\omega_{p_e}}\right)^2 \left[\left(\frac{3.83}{a}\right)^2 - \left(\frac{\omega}{c}\right)^2\right]$, ν is the collision frequency. Depending on the calculation, ν can be either ν_m or ν_{stoc} or the effective collision frequency (see section C). $\omega_{pe} = \sqrt{\frac{e^2 n_e}{\varepsilon_0 m_e}}$ is the electron plasma frequency. Thus, δ is function of applied frequency $f = \omega/2\pi$, plasma electron density n_e and the radius a of the ion source [6]. The geometric effects become important when the skin depth becomes comparable to the size of the driver [6]. When, $a \gg \frac{c}{\omega_{pe}}$, $\omega < \omega_{pe}$ and $\nu < \omega$, then the geometrical effects in the skin depth can be neglected since $x<<1$ and $y\sim1$. This effect was neglected in the previous work [3]. On the contrary, it is taken into account in this paper (see section III.B), since the above indicated inequalities are far from being fulfilled for the NIO1 case. In addition, considering the finiteness of the plasma within the chamber, it was also discovered that the geometrical affect can be important [19].

The stochastic heating collision frequency ν_{stoc} is identified by solving the set of equations described in reference [6]. A pivotal parameter α is necessary for solving these equations and is described in equation (4)

$$\alpha = \frac{4\delta^2\omega^2}{\pi v_{th}^2} \propto \left(\frac{transit\ time\ through\ \delta}{rf period}\right)^2 \tag{4}$$

Where, $v_{th} = \sqrt{\frac{k_B T_e}{m_e}}$ is the electron thermal velocity. It is discussed in the reference [6] that it is convenient to distinguish two ranges $\alpha \ll 1$ and $\alpha \gg 1$ where ν_{stoc} can be expressed analytically. Therefore, a discontinuity arises in the region where the two ranges do not meet.

C. *Effective Collision frequency and Effective Skin depth*

Vahedi [6] introduced an effective collision frequency ν_{eff} (step. (e) in Fig. 1) which is defined as the sum of the ohmic and stochastic collision frequency [1]. From this, the effective skin depth is calculated (step (f) in Fig. 1) which is then used to calculate the power deposition in the plasma.

D. *Power deposition in the plasma*

The RF coil in the driver produces a variable magnetic field which is responsible for the plasma heating within the driver. The plasma heating mechanisms (ohmic and stochastic heating) lead to identify an equivalent region with the thickness δ (estimated in section B) where the power is absorbed by the plasma. To provide an electrical model of this region it is essential to define the electrical conductance and the geometrical extension of this region. The RF coil length, the plasma radius and the skin depth are represented in Fig. 2. The radial position of the end of the skin depth layer δ marks the size of the plasma radius.

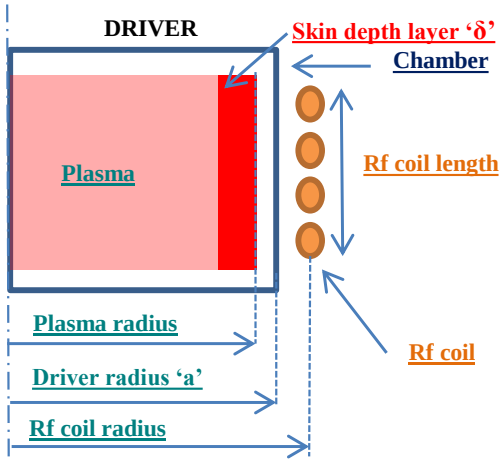

Fig. 2. Schematic of the plasma within the driver

The complex electrical conductivity σ_{el} (step (g) in Fig. 1) of the plasma is defined as follows [1]:

$$\sigma_{el} = \sigma_{el}^{Re} + i\sigma_{el}^{Im}$$
$$\sigma_{el} = \frac{\varepsilon_0 \omega_{pe}^2}{\nu_{eff}^2 + \omega^2}\nu_{eff} + i\frac{(-1)\varepsilon_0 \omega_{pe}^2}{\nu_{eff}^2 + \omega^2}\omega \tag{5}$$

Where, σ_{el}^{Re} and σ_{el}^{Im} are the real and the imaginary part of the plasma conductivity. The two parameters δ and σ_{el}, along with the ν_{eff} are used to calculate the power deposition within the plasma (step (h) in Fig. 1).

The simplified approach to evaluate the power absorbed in the plasma is indicated in the left side of the diagram in Fig. 1; it is the transformer model (see section D.1). On the right side of the diagram is indicated the improved approach to better describe the real experimental geometry of the ion source; it is described by the multi-filament model (see section D.2).

D.1. *The transformer model*

This model is based on the classical approach to represent the plasma and its coupling with the RF coil, as described by Piejak et al [4]. In this model, the driver of an ion source including the plasma are regarded as an air transformer with RF coil as the primary of the transformer and the plasma is considered as the one turn secondary, see Fig. 3.

The classical model does not consider the surrounding metallic structure. On the contrary, in our transformer model, it is assumed that the power transfer efficiency ξ [18] (step (j) in Fig. 1) can be defined as the ratio of the power absorbed by the plasma P_{abs} and the total input power P_{in} and can be given as:

This article has been accepted for publication in a future issue of this journal, but has not been fully edited. Content may change prior to final publication. Citation information: DOI 10.1109/ACCESS.2018.2829618, IEEE Access

$$\xi = \frac{P_{abs}}{P_{in}} = \frac{R_{peq}\, I_{coil}^2}{R_L I_{coil}^2} = \frac{R_{peq}}{R_L}$$

$$\xi = \frac{1}{R_L}\left(R_P \frac{\omega^2 L_{12}^2}{\omega^2 (L_{22}+L_P)^2 + R_P^2}\right) \quad (6)$$

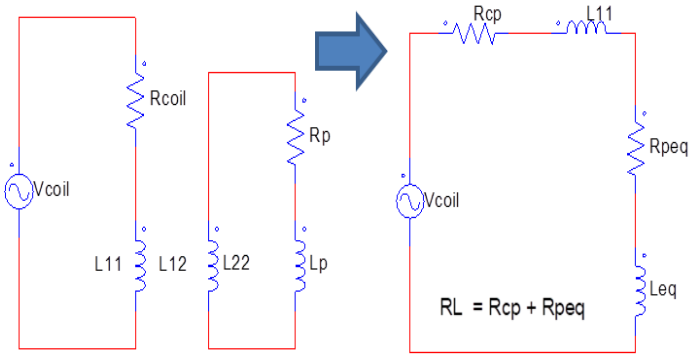

Fig. 3. Transformer model (left hand side) - Equivalent electrical scheme of the driver (right hand side) including the plasma

Where, R_{peq} is the plasma equivalent resistance (step (i) in Fig. 1) at the primary side; $R_{peq} = R_L - R_{cp}$ with R_L as the whole load resistance seen by the generator and R_{cp} as an equivalent resistance accounting for the coil and the metallic structures. L_{12} is the mutual inductance between the coil and the plasma, $L_{11}$and L_{22} are the self-inductance of the coil and the plasma respectively and are calculated from the geometrical dimensions (radius and length) of the plasma and the coil [20]. R_P and L_P are the plasma resistance and inductance. V_{coil} is the voltage across the coil. The plasma length is taken equal to the coil length and the plasma radius is taken equal to the chamber radius, as a first approximation.

D.2. Multi-filament model

In order to apply the methodology presented in the following, the driver should feature geometrical axis symmetry of its conducting parts. The approach is to transform the original 3D electromagnetic problem into a simplified 2D axisymmetric problem to be solved in harmonic regime and quasi magneto-static approximation. Capacitive coupling between the parts is considered negligible in this approximation.

It has been chosen to analyze the 2D problem with the equivalent circuital model approach, described in the following, in order to provide a logical extension of the concept already presented in the previous transformer model approach.

In the 2D model, the conductors (the RF coil, the plasma and the passive metallic structure) are divided into N user-defined, current filaments. The model can be further simplified by considering that the current in passive conductors and plasma at the frequency of interest for this study is significant only on the surface due to the skin effect. In this view the approach is to consider filaments only on the surface and assign to them an effective area calculated considering the geometrical extension of the filament along the surface and the skin depth at the assigned frequency. In Fig. 4 an example of the 2D representation of the multi-filament model for NIO1 ion source is shown. Each of these filaments represents a ring of material whose electric properties are described by a resistance R_i, inductance L_i and mutual inductance M_{ij} with all the other filaments. The electrical equations to solve the problem resemble the set of equations of multiple mutually-coupled inductors, with usual sign convention for passive components, in harmonic regime at the frequency $\omega = 2\pi f$ and can be written as follows:

$$\begin{aligned} U_1 &= (R_1 + j\omega L_1)I_1 + j\omega M_{12} I_2 + j\omega M_{13} I_3 + \cdots + j\omega M_{1N} I_N \\ U_2 &= j\omega M_{21} I_1 + (R_2 + j\omega L_2) I_2 + j\omega M_{23} I_3 + \cdots + j\omega M_{2N} I_N \\ &\vdots \qquad\qquad \ddots \qquad\qquad \ddots \qquad\qquad \vdots \\ U_N &= j\omega M_{N1} I_1 + j\omega M_{N2} I_2 + j\omega M_{N3} I_3 + \cdots + (R_N + j\omega L_N) I_N \end{aligned} \quad (7)$$

Here, the filament resistance R_i and self-inductance L_i at radial position r_i are given as:

$$R_i = \frac{\rho_i 2\pi r_i}{A_{i_{eff}}} \qquad L_i = \mu_0 r_i \log\left(\frac{8r_i}{a} - 2\right) \quad (8)$$

A_{ieff} is the effective area of current filament, μ_0 is the magnetic permeability of vacuum and ρ_i is the resistivity of each filament.

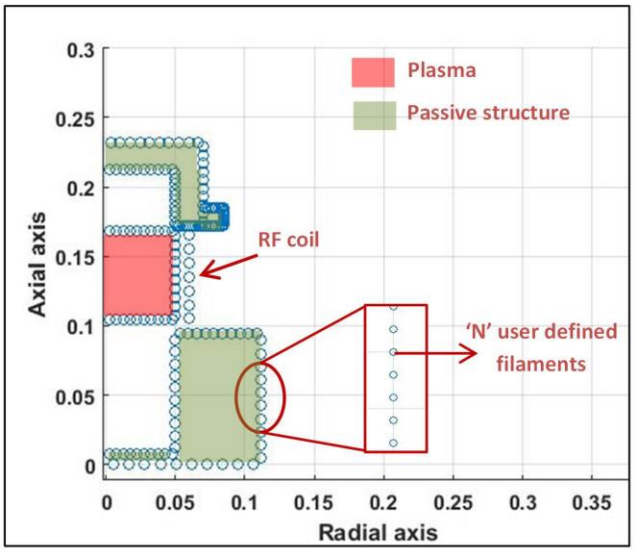

Fig. 4 : Representation of the 2D multi-filament model with 'N' user defined current filaments for the driver of NIO1 ion source

M_{ij} is the mutual inductance between the two filaments at radius r_i, r_j and at the distance d_{ij} and it is defined as follow [21], [22]:

$$M_{ij}(m) = 2\mu\left(\frac{\sqrt{r_i r_j}}{m}\right)\left[\left(1 - \frac{m^2}{2}\right)K(m) - E(m)\right]$$

$$\text{with} \quad m = \sqrt{\frac{4 r_i r_j}{(r_i + r_j)^2 + dij^2}} \quad (9)$$

This article has been accepted for publication in a future issue of this journal, but has not been fully edited. Content may change prior to final publication. Citation information: DOI 10.1109/ACCESS.2018.2829618, IEEE Access

Here, K and E are elliptical integrals of m. To estimate the filament resistance, in the case of plasma, the same complex electrical conductivity σ_{el} is used as described in section D.

Each turn of the RF coil is described as a single filament (with corresponding $U_i = \frac{V_{coil}}{number\ of\ turns\ in\ coil}$)) and the same current is impressed on each of them. In particular, it is worth noting that the filaments representing the plasma and the passive structures are closed in short circuit and the corresponding U_i is set to zero.

By assuming a known value for the impressed current I_{coil} in the RF coil filaments, the currents I_i in the plasma and passive structure filaments can be calculated. From these currents and the calculated resistances, the power dissipated in each filament, thus the power in the coil P_{coil}, plasma P_{abs} and passive structures P_{ps} can be obtained. The power transfer efficiency ξ (step (j) in Fig. 1) in this case is given as:

$$\xi = \frac{P_{abs}}{P_{in}} = \frac{P_{abs}}{P_{coil} + P_{plasma} + P_{ps}} \tag{10}$$

With the known coil current I_{coil}, the equivalent series plasma resistance R_{peq} (step (i) in Fig. 1) and the passive structure resistance $R_{eq_{ps}}$ at the coil side are given as:

$$R_{peq} = \frac{P_{abs}}{I_{coil}^2} \qquad R_{eq_{ps}} = \frac{P_{ps}}{I_{coil}^2} \tag{11}$$

Thus, the power transfer efficiency takes the following form:

$$\xi = \frac{R_{peq}}{R_{coil} + R_{peq} + R_{eq_{ps}}} = \frac{R_{peq}}{R_{peq} + R_{cp}} = \frac{R_{peq}}{R_L} \tag{12}$$

Here, R_L is the whole load resistance seen by the generator and R_{cp} is an equivalent resistance accounting for the coil and the passive metallic structures.

From the calculated values of the current, the magnetic field can also be calculated and the magnetic field lines within the driver will also be represented along with the results.

III. Application to the NIO1 ion source

The methodology described in the previous section is now applied to the driver of the NIO1 ion source operating with the hydrogen gas. A photo of the NIO1 experimental facility is shown in Fig. 5.The schematic of the driver is shown in the Fig. 6. NIO1 has a small RF negative ion source where the inner surface of the source is made up of copper material and covered by molybdenum liners except in the middle where an alumina cylinder isolates the region in vacuum from the RF coil. Permanent magnets in multi-cusp configuration are mounted in the source body to confine the plasma and to reduce plasma losses.

In the following sections, the input parameters, the ohmic and stochastic heating collision frequency and finally the plasma equivalent resistance and power transfer efficiency obtained from the two models (transformer and multi-filament) will be presented.

A. *Input parameters*

The geometrical parameters and the plasma quantities for the driver of the NIO1 ion source are listed in TABLE 1.

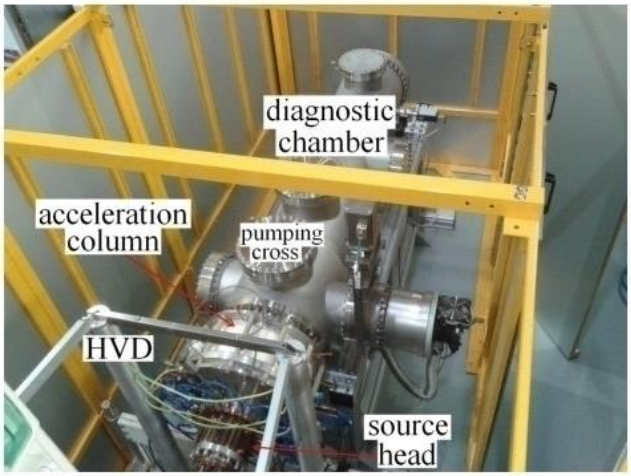

Fig. 5. NIO1 experimental facility (here HVD stands for high voltage deck) [16]

TABLE 1
NIO1 DRIVER PARAMETERS

Geometrical parameters	**Value**
Chamber radius [mm]	50
Number of coil turns	7
Coil radius [mm]	59.5
Solenoid coil length[mm]	63.8
Plasma characteristics	
Gas type	Hydrogen
Electron density, n_e [m^{-3}]*	$\sim 2.1 \times 10^{17}$
Electron temperature, T_e [eV]**	< 7
Gas Pressure, P_{gas} [Pa]	Above 1 Pa
Gas temperature, T_g [K]	400-500

* and ** are taken from [23] and depends upon P_{gas} , $T_{gas}$and B field in the source

A.1. Electron temperature

An estimation of the electron temperature within the driver region of NIO1 ion source is obtained as a function of gas pressure and temperature (see section II.A.1) and is shown in Fig. 7.

This article has been accepted for publication in a future issue of this journal, but has not been fully edited. Content may change prior to final publication. Citation information: DOI 10.1109/ACCESS.2018.2829618, IEEE Access

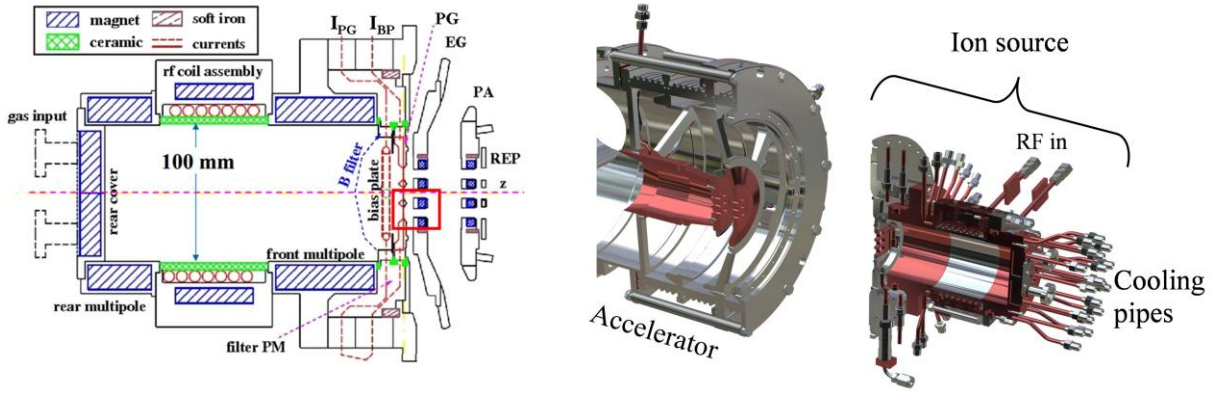

Fig. 6. NIO1 ion source: schematic (left) and 3D drawing cut-view (right) of the driver and the accelerator region

It can be seen that T_e decreases with the increase in pressure P_{gas} for all the gas temperatures T_{gas}. The same trend is also observed in other ion source of similar type [24]. From Fig. 7, we see that at 400 K and at the pressure of 2.5 Pa, T_e is around 3.5 eV and is used as one of the input parameters of the developed methodology.

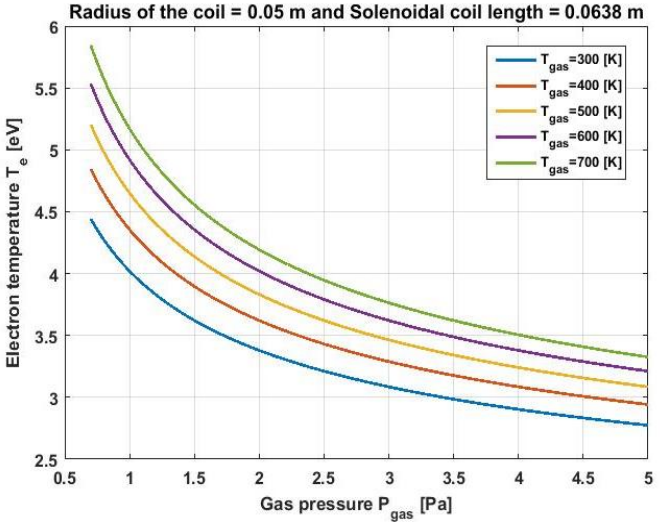

Fig. 7. Estimation of electron temperature with gas pressure

A.2. Electron density

In [23], it is shown experimentally that electron density is about 2×10^{17} m^{-3} at the edge of the driver region of NIO1 ion source. This electron density is measured at the RF power of 1 kW and gas pressure of 1.5 Pa with a negligible magnetic field. In this work, four electron densities n_e from $(1-4) \times 10^{17}$ m^{-3} are taken, in order to observe the trend of the results with the density variation.

B. Effective collision frequencies and skin depth

As explained in the methodology, the input parameters are used to estimate the ohmic, ν_m and the stochastic heating ν_{stoc} collision frequencies. Based on this the effective collision frequency ν_{eff} is calculated (see section II.C) and is shown in Fig. 8.

Fig. 8(a) shows the variation of ν_{eff} ~~(the black curve)~~, ν_m ~~(the red curve)~~ and ν_{stoc} ~~(blue curve)~~ with the gas pressure at the frequency of 2 MHz, $n_e = 3 \times 10^{17}$ m^{-3} and $T_e =$ 3.5 eV (typical operating parameters). It can be seen that stochastic heating is dominant heating mechanism at low pressures (below 1 Pa), whereas ohmic heating is dominant at higher pressures (yellow area). The dominance of stochastic heating at low pressure is in accordance with various research articles [1],[6],[25]–[27]. It can be seen that ν_{stoc} is independent of the pressure variation and depends only on n_e and T_e, while ν_m increases with the increase in pressure. It is pointed out that ν_{stoc} is modeled based on the assumption that the ions do not respond to the RF fields. However, this assumption may not be true for hydrogen gas at 2 MHz; in this case, the ion plasma frequency is found to be higher than the applied frequency. Nevertheless, the electron plasma frequency is found to be much larger than the ion plasma frequency and therefore as a first order approximation ion plasma frequency can be neglected [1].

From the input parameters and the effective collision frequency ν_{eff}, the effective skin depth is calculated from equation (3) and the results are shown in Fig. 8(b) and Fig. 9. Usually, when the radius of the chamber is large, then the geometric effects present in equation (3) are neglected. However, for the smaller chamber these effects should be taken into consideration [6] [19]. In Fig. 8 (b), the skin depth variation is shown for two conditions (with and without geometric effect) as a function of frequency. Without the consideration of the geometric effect, it can be seen that the skin depth increases with the decrease in frequency, reaching comparable values with the driver radius. This certainly does not represent a physical scenario. Conversely, considering the geometric effects it can be seen that the increase in skin depth is minimal with respect to the decrease in frequency. This is in accordance with [19] where it is shown that due to the finiteness of the plasma within the driver, the skin depth does not increase very much even at the low frequencies.

This article has been accepted for publication in a future issue of this journal, but has not been fully edited. Content may change prior to final publication. Citation information: DOI 10.1109/ACCESS.2018.2829618, IEEE Access

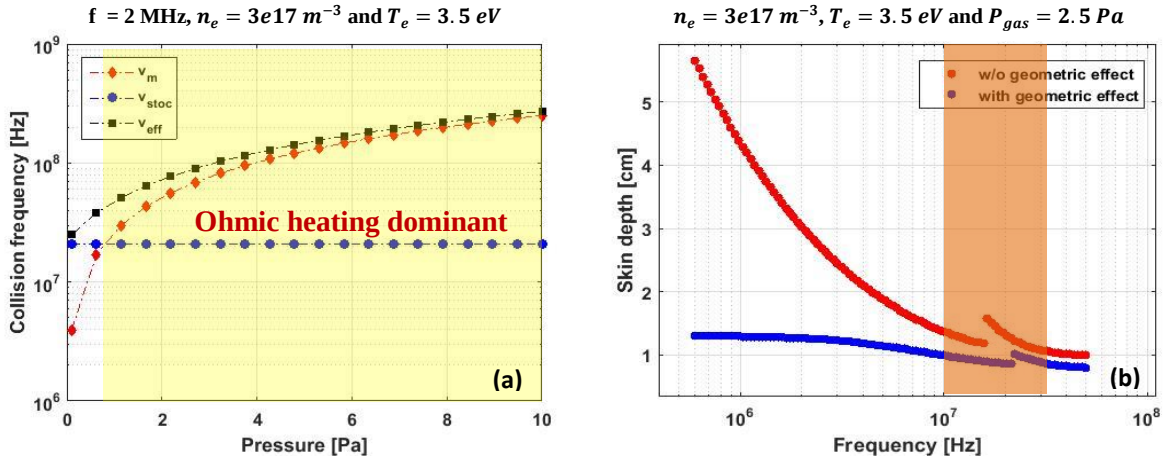

Fig. 8. Variation of (a) effective, ohmic and stochastic collision frequency with gas pressure and (b) skin depth with applied frequency

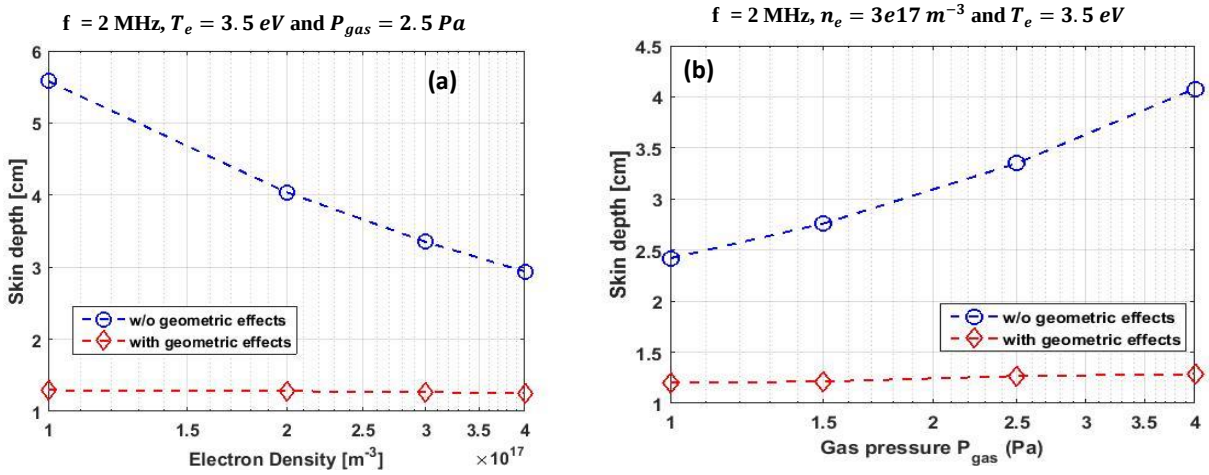

Fig. 9. Skin depth variation with (a) electron density and (b) gas pressure

A discontinuity in the skin depth curves highlighted in the orange region in Fig. 8 (b) appears because of the model considered for ν_{stoc}, where the solution for ν_{stoc} is available as a limit for two disjoint regimes.

The frequency range of 0.6-50 MHz is chosen for the analyses because within this range the frequencies 1, 2 and 13.56 MHz are present. The 1 and 2 MHz are the working frequency of the ITER ion source and NIO1 ion source and 13.56 MHz is the standard working frequency of ICPs in general. We limit the upper frequency range to 50 MHz because above this frequency other phenomena like ion - ion collisions may start playing an important role in plasma heating, which is not taken into account in the model.

The variation of skin depth with and without geometrical effects for different electron densities and gas pressures is shown in Fig. 9. Without the geometric effects, the skin depth decreases with the increase in density, (Fig. 9(a)), this is because $\delta \propto \frac{1}{\sqrt{n_e}}$ (see equation (3)). On the other hand, the skin depth increases with the increase in gas pressure (Fig. 9 (b)) because ν_{eff} increases with the increase in gas pressure, see Fig. 8(a). It can be seen that considering the geometric effects the skin depth reduces considerably from about 5.5 cm at low electron density and about 4 cm at high gas pressure (which is comparable to the radius of the source) to about 1.2 cm. The effect of electron density and gas pressure on the skin depth is less prominent when geometric effects are considered. In the following section, the results are shown considering the geometric effects, thus applying equation (3).

C. Power transfer to the plasma

The methodology described in section II is applied to the NIO1 ion source to calculate the plasma equivalent resistance (PER), R_{peq} and the power transfer efficiency (PTE) ξ. Both the first and the improved approach are applied and are described in the following sections.

C.1. Transformer model

As described in section II.D.1, the "classical" transformer model is considered with some improvements. The equivalent electrical scheme of the driver of the NIO1 ion source is

shown in Fig. 3. R_{cp} is taken to be varying proportional t $f^{\frac{1}{2}}$o, a reasonable choice considering the small skin depth with respect to the conductor thickness. At 2 MHz, R_{cp} is assumed to be 0.3 Ω.

C.2. Multi-filament model

The 2D axis symmetrical geometry of the full NIO1 driver, shown in Fig. 6, along with the passive metallic structure is built in MATLAB® (Fig. 10) and is used as an input for the multi-filament model (described in section II.D.2). Furthermore, in order to reduce the model complexity and the computational time, the exploitation of the skin effect present in harmonic regime has been considered with a simplified approach, namely considering only a single layer of filaments on the surface of the metal parts. These filaments are visible in Fig. 10 as blue circles located at the surface of the conductors. An example of the magnetic field lines within the driver region are also represented in Fig. 10 when applying an I_{coil} impressed current of 1 A.

D. Results

The results of the application of the methodology to the NIO1 ion sources are first shown as a function of frequency $f = \frac{\omega}{2\pi}$; then, the focus is more on the operating parameters of the NIO1 ion source at the working frequency of 2 MHz. The relative merit of the multi-filament model against the transformer one is presented. In all these cases, the plasma radius is assumed to be the same as the chamber radius. Finally, the results are also shown for a scan with respect to the equivalent plasma radius.

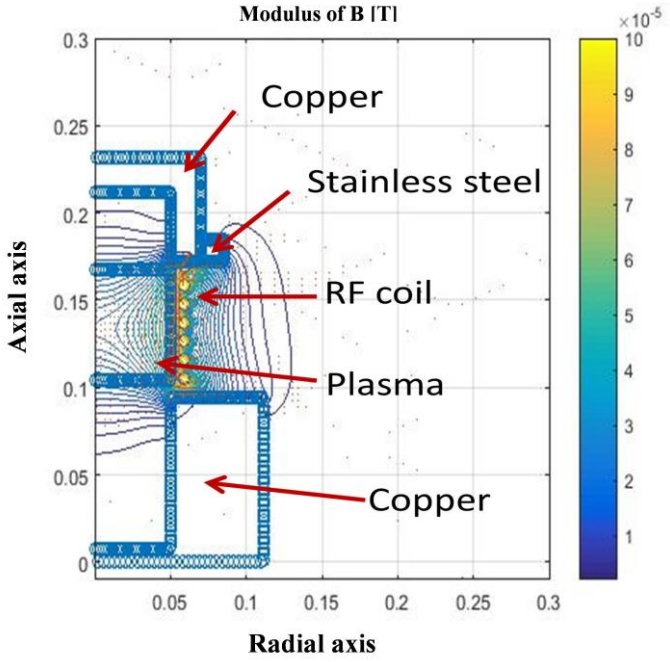

Fig. 10. Schematic of the 2D axis-symmetry model of the driver of the NIO1 ion source

D.1. Application of the transformer model – PER and PTE versus frequency

- *Plasma equivalent resistance at the primary side of the coil*

The value of the plasma equivalent resistance is calculated (as shown in equation (6)) at different frequencies f and plotted in Fig. 11. It can be noticed that at 2 MHz, PER is found to be about 9 Ω for typical values for NIO1 operation. In these plots, we can see that the value of PER obtained is first increasing with the increase in frequency, reaches a maximum value and then decreases with the further increase in frequency. A discontinuity arises as explained in section B due to the modelling of the stochastic heating collision frequency v_{stoc}, this discontinuity is shown with an interpolation (dashed line) in Fig. 11 and Fig. 12. The results obtained in this range may not be reliable.

With the density variation, see Fig. 11(a), the PER increases with the increase in density. All the measurement results provided in [28] indicate a monotonic increase with electron density, which is also the frequently reported result. With the pressure variation (see Fig. 11(b)), the analyses show that at lower frequencies, the PER decreases with the increase in pressure whereas at higher frequencies the PER increases with the increase in pressure. This trend of the increase of the resistance with the increase of pressure is also observed in [28]. It should be noted that the gas used in [28] is a noble gas and here we use hydrogen gas, which has a very different electron-neutral collision frequency as compared to a noble gas.

- Power transfer efficiency

The value of power transfer efficiency ξ at different frequencies f is calculated and plotted in Fig. 12. In these plots we can see that ξ increases with the increase in frequency and then reaches a maximum value. At low frequency and low density, the PTE reaches as low as 65% whereas at high frequency it reaches as high as 97%. With respect to the density or pressure variation, PTE in Fig. 12(a) and (b), show similar trend as is seen with the PER, in Fig. 11.

D.2. Application of the multi-filament model and comparison with the transformer one

- PER and PTE versus frequency

Fig. 13 shows a comparison between the results of both transformer and filament models for the typical operational parameters for NIO1 ion source as a function of frequency. It can be seen that with the multi-filament model both PER and PTE follows the same trend as that of transformer model. The PER obtained from multi-filament model is reduced by half as compared to the transformer model, whereas the PTE is reduced by 2 %, with an exception at low frequency where it is reduced considerably by about 18 %. At lower frequencies, the value of PTE is lower as compared to the value at higher frequencies; this is because at lower frequencies the PER is

This article has been accepted for publication in a future issue of this journal, but has not been fully edited. Content may change prior to final publication. Citation information: DOI 10.1109/ACCESS.2018.2829618, IEEE Access

comparable to the resistance of passive metallic structure.

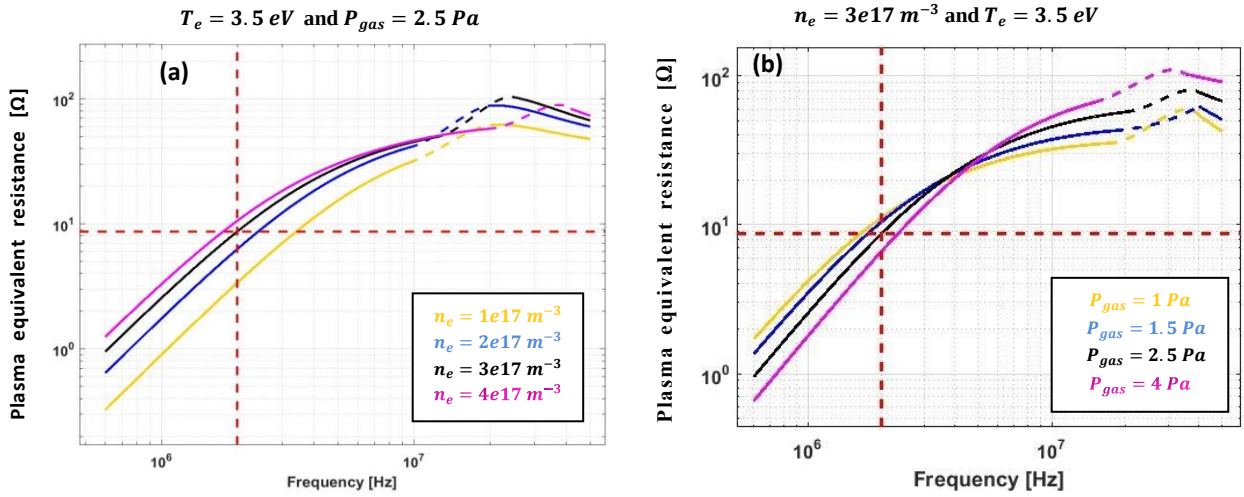

Fig. 11. Variation of plasma resistance with frequency for different (a) electron density and (b) gas pressure

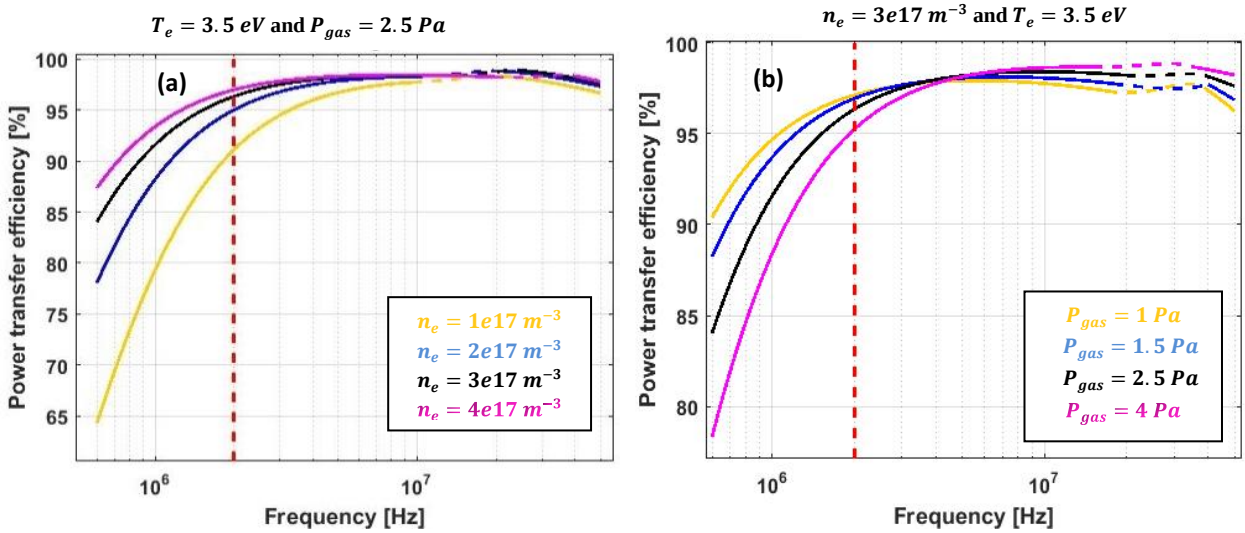

Fig. 12. Variation of power transfer efficiency with frequency for different (a) electron densities and (b) gas pressure

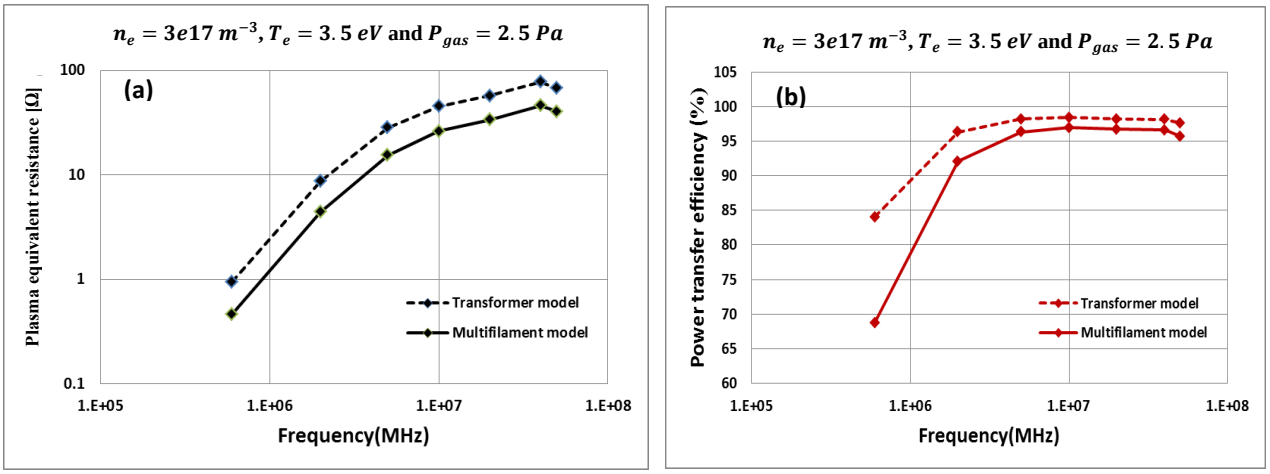

Fig. 13. (a) Plasma equivalent resistance variation with frequency and (b) Power transfer efficiency variation with frequency

This article has been accepted for publication in a future issue of this journal, but has not been fully edited. Content may change prior to final publication. Citation information: DOI 10.1109/ACCESS.2018.2829618, IEEE Access

However, as the frequency increases, the PER becomes much larger than the resistance of the passive metallic structure and thus negligible power is dissipated in the metallic structure.

- PER and PTE versus electron density

The value of PER and PTE for different electron densities is plotted in Fig. 14. In this graph, it can be seen that both PER and PTE increases with the increase in electron density. The same behavior of PER is also observed experimentally in [28] for different inert gases like He, Ne, Ar and Kr. The PER estimated from the multi-filament model is roughly half the value obtained from the transformer model. The PTE reduces by 4% for high electron density and about 10% for low electron density.

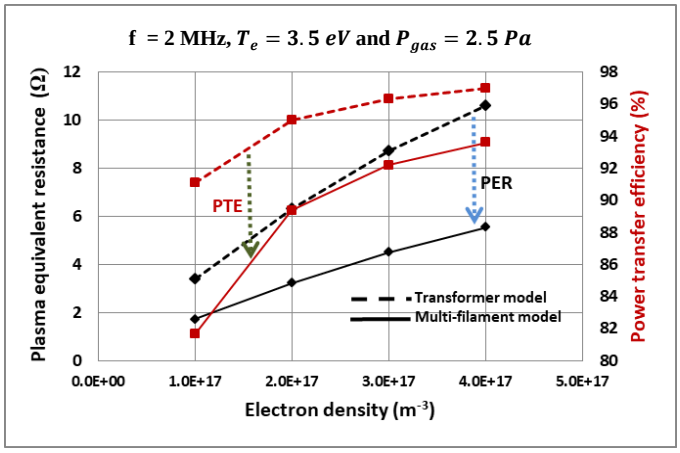

Fig. 14. Plasma equivalent resistance and power transfer efficiency variation with electron density

- PER and PTE versus gas pressure

The value of PER and PTE for different gas pressure is plotted in Fig. 15. The PER estimated from the multi-filament model is roughly half the value obtained from the transformer model. The PTE reduces by 4% for low gas pressure and about 6% for high gas pressure.

In this graph, it can be seen that both PER and PTE decrease with the increase in gas pressure. The behavior of PER is different from what is observed experimentally in [28] for different inert gases like Ne, Ar and Kr. However, for He the same behavior is seen at higher gas pressure above 2.6 Pa. A possible interpretation of the discrepancies between the results obtained from the noble gases and hydrogen is that they could be due to the different electron neutral collision frequency in Hydrogen and in noble gases.

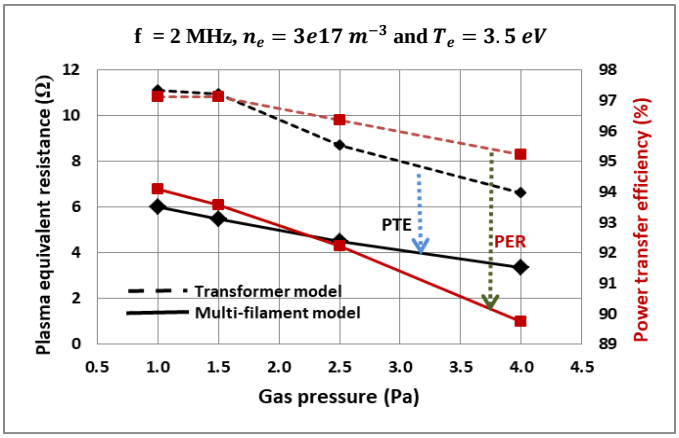

Fig. 15. Plasma equivalent resistance and power transfer efficiency variation with gas pressure

- PER and PTE versus the plasma radius

The results obtained in the previous sections are calculated by considering the uniform electron density within the plasma chamber. However it has been observed experimentally that the plasma electron density is not uniform in the entire chamber region; it follows a profile showing a maximum at the center and decreasing values near the edges [29]. This implies that the plasma conductivity is not uniform within the chamber. The plasma in the inner region is more conducting than that in the outer region. So as a first approximation, the outer region is considered non-significant and a radial step-wise density profile is assumed. The equivalent plasma resistance can be calculated for an intermediate value of the radius. Since the plasma equivalent resistance calculated from the multi-filament model can be considered more realistic than that obtained from the transformer model, in this section the results are presented only for the multi-filament model. A scan with respect to the plasma radius (from 5-2 cm) is presented in Fig. 16 at 2 MHz and for typical values of NIO1 operation. It is pointed out that consideration of such unrealistic range for the variation of the plasma equivalent radius is done only to see its effect on the trend of the results obtained.

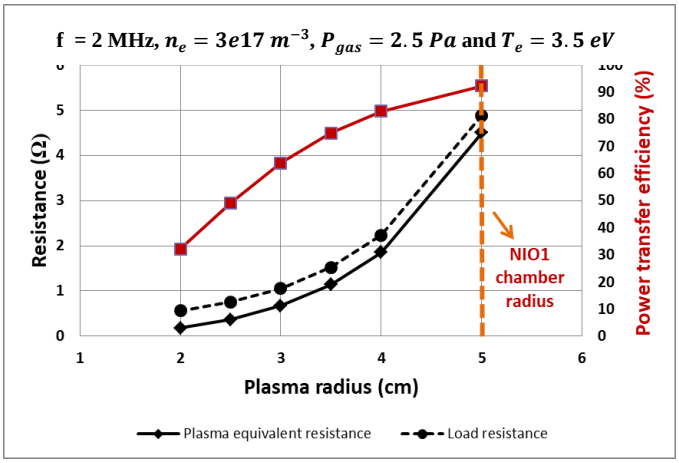

Fig. 16. Plasma equivalent resistance, load resistance and power transfer efficiency variation with plasma radius using multi-filament model

The reduction of the equivalent plasma radius within the chamber suggests a reduction in the PER and PTE. The PER reduces from about 4.5 Ω at 5 cm plasma radius to about 0.18 Ω at the plasma radius of 2 cm. The PTE decreases by 60% in reducing the plasma radius from 5 cm to 2 cm.

The load resistance R_L is calculated using the relation shown in equation (12) and is also shown in Fig. 16. It follows the same trend as that of PER. In [30], an estimation of the load resistance (RF coil, passive structures and plasma) of 1.7 Ω is given for NIO1 ion source. This value of R_L is found at a plasma radius of 3.5 - 4 cm from the methodology presented in this paper.

IV. Conclusion and Future Work

This paper provides an improved methodology to estimate the plasma equivalent resistance and the power transfer efficiency within the driver region of an IC ion source. The major improvement with respect to a previous methodology based on a simpler transformer model comes from the development of a multi-filament model which takes into account the mutual coupling between the RF coil, the plasma and the metallic structure within the driver region. Both the methodologies are applied to the NIO1 ion source.

With the transformer model, it is found that the plasma equivalent resistance is about 9 Ω at the NIO1 operating frequency of 2 MHz. With the implementation of the multi-filament model, it is found that the plasma equivalent resistance reduces to about half the value obtained from the transformer model and the PTE reduces by 4% for the typical values of NIO1 operation. These results seem corresponding to a more realistic description of the real phenomena. In addition, the assumption of a reduced equivalent plasma radius, accounting in some way for a more realistic density profile leads to an evaluation of plasma equivalent resistance closer to the estimated value.

From both models, it can be seen that the power transfer efficiency increases with the increase in operating frequency reaching maximum values around 10 MHz, thus, this indicates that the preferable operating frequency lies in this range.

As a future work, the developed methodology could be made more self-consistent, in such a way that plasma parameters like electron density and temperature are not considered independently. Future calculations of the radial density profile could also be included. The external static magnetic field applied in ion source to confine plasma away from the wall chamber is expected to have an impact on the plasma conductivity. Therefore, it will be interesting to incorporate this effect into the methodology and hence obtain the results in view of more realistic experimental scenario.

References

[1] M. A. Lieberman and A. J. Lichtenberg, *Principles of Plasma Discharges and Materials Processing*, Second Edi. A John wiley & sons, inc publication, 2005.

[2] P. Chabert and N. Braithwaite, *Physics of Radio-Frequency Plasmas*. 2011.

[3] P. Jain *et al.*, "Evaluation of power transfer efficiency for a high power inductively coupled radio-frequency hydrogen ion source," *Plasma Phys. Control. Fusion*, vol. 60 045007, 2018.

[4] R. B. Piejak, V. Godyak, and B. M. Alexandrovich, "A simple analysis of an inductive RF discharge," *Plasma Sources Sci. Technol.*, vol. 1, pp. 179–186, 1992.

[5] V. Godyak, "Electrical characteristics and electron heating mechanism of an inductively coupled argon discharge," *Plasma Sources Sci. Technol.*, vol. 3, pp. 169 – 176, 1994.

[6] V. Vahedi, M. A. Lieberman, G. Dipeso, T. D. Rognlien, and D. Hewett, "Analytic model of power deposition in inductively coupled plasma sources," *J. Appl. Phys.*, vol. 78, no. 3, pp. 1446–1458, 1995.

[7] V. A. Godyak, R. B. Piejak, and B. M. Alexandrovich, "Experimental setup and electrical characteristics of an inductively coupled plasma," *J. App. Phys.*, vol. 85, no. 2, pp. 703–712, 1999.

[8] K. Suzuki, K. Nakamura, H. Ohkubo, and H. Sugai, "Power transfer efficiency and mode jump in an inductive RF discharge," *Plasma Sources Sci. Technol.*, vol. 7, no. 1, pp. 13–20, 1998.

[9] M. Cavenago and S. Petrenko, "Models of radiofrequency coupling for negative ion sources Models of radiofrequency coupling for negative ion sources a)," *Cit. Rev. Sci. Instruments*, vol. 83, pp. 2–503, 2012.

[10] U. Fantz, P. Franzen, and D. Wünderlich, "Development of negative hydrogen ion sources for fusion: Experiments and modelling," *Chem. Phys.*, vol. 398, no. 1, pp. 7–16, 2012.

[11] "ITER official website." [Online]. Available: http://www.iter.org/.

[12] R. S. Hemsworth *et al.*, "Neutral beams for ITER (invited)a)," *Rev. Sci. Instrum.*, vol. 67, no. 3, p. 1120, 1996.

[13] B. Heinemann *et al.*, "Negative ion test facility ELISE—Status and first results," *Fusion Eng. Des.*, vol. 88, no. 6–8, pp. 512–516, 2013.

[14] D. Marcuzzi, P. Agostinetti, M. Dalla Palma, H. D. Falter, B. Heinemann, and R. Riedl, "Design of the RF ion source for the ITER NBI," *Fusion Eng. Des.*, vol. 82, no. 5–14, pp. 798–805, 2007.

[15] M. Cavenago *et al.*, "Development of versatile multiaperture negative ion sources," *AIP Conf. Proc.*, vol. 1655, no. 2015, p. 40006, 2015.

[16] M. Cavenago *et al.*, "First experiments with the negative ion source NIO1," *Rev. Sci. Instrum.*, vol. 87, no. 2, pp. 1–5, 2016.

[17] M. Tuszewski, "Particle and heat transport in a low-frequency inductively coupled plasma," *Cit. Phys. Plasmas*, vol. 5, 1998.

[18] M. Cazzador, "Analytical and numerical models and first operations on the negative ion source NIO1," Università degli studi di padova, 2014.

[19] A. U. Rehman and Y. K. Pu, "Effect of boundary conditions on the classical skin depth and nonlocal behavior in inductively coupled plasmas," *Phys.*

Plasmas, vol. 12, no. 9, pp. 1–2, 2005.

[20] E. Turkoz and M. Celik, "2D Axisymmetric Fluid and Electromagnetic Models for Inductively Coupled Plasma (ICP) in RF Ion Thrusters," in *33rd International Electric Propulsion Conference*, 2013, pp. 1–9.

[21] S. I. Babic and C. Akyel, "New analytic-numerical solutions for the mutual inductance of two coaxial circular coils with rectangular cross section in air," *IEEE Trans. Magn.*, vol. 42, no. 6, pp. 1661–1669, 2006.

[22] G. Chitarin and M. Guarnieri, "An Integral Formulation for Eddy Current Analyses in Axisymmetric Configurations," *IEEE Trans. Magn.*, vol. 25, no. 5, pp. 4330–4342, 1989.

[23] P. Veltri *et al.*, "Langmuir probe characterization of the NIO1 ion source plasma," in *submission to 17th International Conference on Ion sources - AIP proceedings*, 2017.

[24] J. P. Boeuf, G. J. Hagelaar, P. Sarrailh, G. Fubiani, and N. Kohen, "Model of an inductively coupled negative ion source: II. Application to an ITER type source," *Plasma Sources Sci. Technol*, vol. 20, 2011.

[25] M. M. Turner, "Collisionless Electron Heating in an Inductively Coupled Discharge," *Phys. Rev. Lett.*, vol. 71, no. 12, pp. 1844–1847, 1993.

[26] M. A. Lieberman and V. A. Godyak, "From Fermi acceleration to collisionless discharge heating," *IEEE Trans. Plasma Sci.*, vol. 26, no. 3, pp. 955–986, 1998.

[27] G. P. Canal, H. Luna, and R. M. O. Galvão, "Characterization of the transition from collisional to stochastic heating in a RF discharge," *J. Phys. D. Appl. Phys.*, vol. 43, no. 2, p. 25209, 2010.

[28] E. A. Kralkina *et al.*, "RF power absorption by plasma of a low-pressure inductive discharge," *Plasma Sources Sci. Technol.*, vol. 25, no. 1, p. 15016, 2016.

[29] M. Tuszewski, "Enhanced Radio Frequency Field Penetration in an Inductively Coupled Plasma.," *Phys. Rev. Lett.*, vol. 77, no. 7, pp. 1286–1289, 1996.

[30] M. Cavenago *et al.*, "Construction of a versatile negative ion source and related developments," *AIP Conf. Proc.*, vol. 1515, no. 1, pp. 157–166, 2013.

Palak Jain was born in 1990, received the B.Sc degree in physics hons from St. Stephens College, University of Delhi, India in 2008. She was a part of the dual degree master's program between University of Paris Sud 11 and University of Delhi. Thus receiving M.Tech in Nuclear Science and Technology in 2014 from University of Delhi, India and M.S. in Nuclear Reactor Physics and Engineering in 2013 from University of Paris Sud 11, France. Currently, she is an Erasmus Mundus Fusion Dc - Ph.D. student enrolled in the Joint European research doctorate in Fusion Science and Engineering at Consorzio RFX, Padova, Italy since 2014. Her research interest includes the studies of RF power circuits for negative ion sources for neutral beam injectors; the study of the plasma sources; its behavior and efficiency.

Mauro Recchia was born in 1976. He graduated in electronic engineering from University of Padova, Italy, in 2004, and receives the Ph.D degree in electrical engineering in 2009. He is a researcher with Consorzio RFX and a member of the Power System group. He is responsible officer of the power supply system for MHD control of the RFX experiment and work package manager of the electrical modeling of the SPIDER project of the ITER Neutral Beam test Facility under construction in Padova. His research interest includes high power switching converters for fusion experiments, modelling of high voltage circuits for fast transient studies, modelling of high power radio frequency circuits for inductively coupled plasma sources, computational electromagnetics.

Pierluigi Veltri received the B.S in physics from the Università degli Studi della Calabria, Italy, in 2004 and M.S. degrees in astrophysics and plasmas in 2006. In 2011 he received the European joint Ph.D. degree in Fusion Science and Engineering, from the Padova University (Italy) and Istituto Superior Tecnico (Portugal). From 2011 to 2012, he was post-doc at Padova University. He was then selected for an EFDA (European Fusion Development Agreement) Fellowship, carried out from 2012 to 2014. From 2015 to 2017 he was a researcher at the INFN (Istituto Nazionale di Fisica Nucleare) at LNL (Legnaro National Laboratory), Italy. Since 2017 he is researcher at Consorzio RFX, Padova, Italy. His research interests includes modelling of high power neutral beam injectors for plasma heating in magnetic confinement fusion device, low temperature plasmas and radiofrequency ion sources.

This article has been accepted for publication in a future issue of this journal, but has not been fully edited. Content may change prior to final publication. Citation information: DOI 10.1109/ACCESS.2018.2829618, IEEE Access

Marco Cavenago was born in Vimercate, Italy, in 1961. He earned the Laurea degree in physics from Pisa University in 1984 and received the Ph.D. degree in physics from Scuola Normale Superiore in 1987, discussing new techniques in particle acceleration and instabilities in betatrons. He worked on the same subjects at University of California, Irvine, in 1985–1986. Since 1988, he has worked with the Laboratori Nazionali of Legnaro, Italy, a branch of Istituto Nazionale di Fisica Nucleare. His research interests are focused on mathematical physics of particle acceleration, plasma physics, and accurate design of electromagnetic devices of ion sources: magnets, einzel lenses, and microwave or radiofrequency components. The major projects that he has designed are a 14 GHz Electron Cyclotron Resonance ion source, a 350 kV high voltage platform and a nine-beamlet multiaperture 2 MHz negative ion source, which is intended to support the development of neutral beam injectors for fusion in collaboration with Consorzio RFX, Padua (near Legnaro). He also participated towards the development (within collaboration between University of Milan and INFN) of particle traps and beam coolers. He is the author of more than 200 research articles, spanning from experimental results to multi-physics simulations to advanced theoretical studies of particle extraction and complex transport systems, also in space charge dominated regimes.

Alberto Maistrello was born in 1984, graduated in Electric Engineering in 2009 at the University of Padova, Italy and he is currently a Ph.D. student of the Joint European research doctorate in Fusion Science and Engineering. He is with Consorzio RFX since 2010 as researcher in the field of Power Supply engineering for fusion experiments. Specific research fields are power quality in HV and MV grids, dc current interruption, RF circuits for Neutral Beam Injectors ion sources.

Elena Gaio was born in 1958, Dr. degree in Electronic Engineering at University of Padova - Italy in 1983, senior researcher with Consorzio RFX, Power Systems Group Leader, coordinator of Consorzio RFX activities for JT-60SA project in the frame of the Broader Approach Agreement. Field of research: power supply systems for fusion experiments, with particular reference to high-power static converters, dc circuit breakers, switching converters, and relevant controls, neutral beam injectors and relevant radiofrequency ion sources, with particular reference to the electrical and circuital aspects.